Interface Crack Problems in Anisotropic Solids Analyzed by the MLPG

J. Sladek[1], V. Sladek[1], M. Wünsche[2] and Ch. Zhang[2]

Abstract: A meshless method based on the local Petrov-Galerkin approach is proposed, to solve the interface crack problem between two dissimilar anisotropic elastic solids. Both stationary and transient mechanical and thermal loads are considered for two-dimensional (2-D) problems in this paper. A Heaviside step function as the test functions is applied in the weak-form to derive local integral equations. Nodal points are spread on the analyzed domain, and each node is surrounded by a small circle for simplicity. The spatial variations of the displacements and temperature are approximated by the Moving Least-Squares (MLS) scheme. After performing the spatial integrations, one obtains a system of ordinary differential equations for certain nodal unknowns. The backward finite difference method is applied for the approximation of the diffusive term in the heat conduction equation. Then, the system of the ordinary differential equations of the second order resulting from the equations of motion is solved by the Houbolt finite-difference scheme as a time-stepping method.

Keywords: Meshless local Petrov-Galerkin method (MLPG), moving least-squares approximation, anisotropic materials, Houbolt method, backward finite difference method

1 Introduction

Layered or laminated composites composed of dissimilar materials are increasingly applied in engineering structures. Interface failure is one of the most dominant failure mechanisms in laminated structures. Williams (1959), Erdogan (1963, 1965), England (1965), and Sih and Rice (1964, 1965) analyzed the interface crack problems and showed that an oscillation of the stresses or overlapping of crack-faces near the crack-tip occurs although the traction-free boundary conditions are

---

[1] Institute of Construction and Architecture, Slovak Academy of Sciences, 84503 Bratislava, Slovakia, sladek@savba.sk

[2] Department of Civil Engineering, University of Siegen, D-57068 Siegen, Germany

assumed on the crack-faces. Various models, based on an assumption of the existence of a small contact zone [Comninou (1977), Comninou and Schmeser (1979)], or a third material between two bonded materials ahead of the crack-tip [Atkinson (1977)], or a crack-tip with a finite opening angle [Sinclair (1980)], or no-slip zones [Mak et al. (1980)], have been proposed to avoid the above mentioned physically inadmissible phenomena. These models are successful in removing the oscillatory behaviour and contribute to a better understanding of the fracture processes on a bimaterial interface. Yuuki and Cho (1989) pointed out that the oscillation region can be ignored, since that region is extremely small and introduced a unique definition of the stress intensity factors to avoid the original confusion related to the analyses of Erdogan (1963), and Rice and Sih (1965).

The solution of general boundary value problems for transient elastodynamic or thermoelastic problems in anisotropic solids requires advanced numerical methods due to the high mathematical complexity. Several computational methods have been proposed over the past years to analyze thermoelastic problems in homogeneous materials. Shiah and Tan (1999) applied the boundary element method (BEM) for 2-D uncoupled thermoelasticity in anisotropic solids. Particular integral formulations for 2-D and 3-D transient uncoupled thermoelastic analyses have been presented by Park and Banerjee (2002). The BEM has been successfully applied also to coupled thermoelastic problems [Sladek and Sladek (1984); Dargush and Banerjee (1991); Chen and Dargush (1995); Suh and Tosaka (1989); Hosseini-Tehrani and Eslami (2000)]. Dual reciprocity BEM has been presented by Gaul *et al*. (2003), and Kögl and Gaul (2003). In spite of the great success of the finite element method (FEM) and BEM as effective numerical tools for the solution of boundary value problems in mainly elastic solids, there is still a growing interest in the development of new advanced numerical methods. In recent years, meshless formulations are becoming popular due to their high adaptability and low costs to prepare input and output data in numerical analysis. The moving least squares (MLS) approximation is generally considered as one of many schemes to interpolate discrete data with a reasonable accuracy. The order of continuity of the MLS approximation is given by the minimum between the orders of continuity of the basis functions and that of the weight function. So continuity can be tuned to a desired value. In conventional discretization methods, the interpolation functions usually result in a discontinuity in the secondary fields (gradients of primary fields) on the interfaces of elements. Numerical models based on C^1-continuity, such as in meshless methods, are expected to be more accurate than conventional discretization techniques in homogeneous or continuously nonhomogeneous solids. However, higher order continuous primary fields (displacements, temperature) are not able to model jumps for secondary fields (gradients of primary fields) due to disconti-

nuities of the material coefficients on the interfaces of the joint laminates. Therefore, a special treatment for modeling discontinuities for piecewise homogeneous solids is required in case of higher order modeling like in meshless approximation [Li et al. (2003)]. A discontinous Galerkin meshfree formulation is proposed by Wang et al. (2009) to solve the potential and elasticity problems of composite material. The domain is partitioned into subdomains with uniform material properties. The discretized meshfree particles within a subdomain are clarified as one particle group. Various subdomains occupied by different particle groups are then linked using the discontinuous Galerkin formulation where averaged interface traction is constructed based on the tractions computed from the adjacent subdomains. The meshless or generalized FEM methods are also very convenient for modeling cracks. One can embed particular enrichment functions at the crack-tip so the stress intensity factors can be predicted accurately [Fleming et al, (1997)].

A variety of meshless methods has been proposed so far and some of them have been also applied to transient heat conduction problems [Batra et al. (2004); Sladek et al. (2003a,b, 2004a, 2005); Wu at al. (2007)] or thermoelastic problems [Sladek et al. (2001, 2006); Bobaru and Mukherjee (2003)]. They can be derived from a weak-form formulation either on the global domain or on a set of local subdomains. In the global formulation, background cells are required for the integration of the weak-form. In methods based on local weak-form formulation, no background cells are required and therefore they are often referred to as truly meshless methods. The meshless local Petrov-Galerkin (MLPG) method is a fundamental base for the derivation of many meshless formulations, since the trial and the test functions can be chosen from different functional spaces [Zhu et al. (1998); Atluri and Zhu (1998); Atluri et al. (2000); Sladek et al., (2000, 2001, 2003a,b) Sellountos et al., (2005,2009)]. Recently, the MLPG method with a Heaviside step function as the test functions [Atluri et al. (2003); Sladek et al., (2004b, 2006)] has been applied to solve two-dimensional (2-D) homogeneous and continuously nonhomogeneous elastic solids. By using the MLPG, the present authors have recently analyzed 3-D axisymmetric [Sladek et al. (2007)], general 3-D heat conduction [Sladek et al. (2008a)], and plate and shell problems under a thermal load [Sladek et al. (2008b,c)].

In this paper, the MLPG method is applied to solving two-dimensional transient uncoupled thermoelastic problems for an interface crack between two dissimilar anisotropic materials. Two sets of collocation nodes are assigned on both sides of the material interface at the same location but with different material properties. The moving least-squares (MLS) approximation is carried out separately for each of the homogeneous domains, so that the domain of influence is truncated at the interface. The high order continuity is kept within each homogeneous domain, but

not across the interface of the joint domains. In uncoupled thermoelasticity, the temperature field is not influenced by the mechanical displacements. Therefore, the heat conduction equation is solved first to obtain the temperature distribution. The equations of motion are subsequently solved. In the solution procedure, nodal points are introduced and distributed over the analyzed domain, each of which is surrounded by a small circle for 2-D problems. The weak-form on small subdomains with a Heaviside step function as the test functions is applied to derive local integral equations. After performing the spatial MLS approximation, a system of ordinary differential equations for certain nodal unknowns is obtained. The backward finite difference method is applied for the approximation of the diffusive term in the heat conduction equation. Then, the system of the ordinary differential equations of the second order resulting from the equations of motion is solved by the Houbolt finite-difference scheme as a time-stepping method. Numerical examples are presented and discussed to show the accuracy and the efficiency of the present method.

2   Local integral equations

The governing equations of coupled linear thermoelasticity [Nowacki (1986)] take the form

$$\sigma_{ij,j}(\mathbf{x},\tau) + X_i(\mathbf{x},\tau) = \rho \ddot{u}_i(\mathbf{x},\tau), \tag{1}$$

$$[k_{ij}(\mathbf{x})\theta_{,j}(\mathbf{x},\tau)]_{,i} - \rho(\mathbf{x})c(\mathbf{x})\dot{\theta}(\mathbf{x},\tau) - T_o\beta_{ij}(\mathbf{x})\dot{\varepsilon}_{ij}(\mathbf{x},\tau) = 0, \tag{2}$$

where $\ddot{u}_i$, ρ and X_i denote the acceleration of displacements, the mass density, and the body force vector, respectively. The stress field σ_{ij} is influenced not only by the displacement gradients in deformed elastic solids but also by the temperature field distribution, since also a thermal expansion of the solids is contributing to the total strains. The temperature θ is measured from the unstrained value T_o, i.e. $\theta = T - T_o$ and $\varepsilon_{ij} = 0$ when $T = T_o$. Furthermore, k_{ij} and c are the thermal conductivity tensor and the specific heat, respectively, while β_{ij} are the material coefficients accounting for the interaction between the strain and the temperature fields. A comma after a quantity represents the partial derivatives of the quantity and a dot is used for the time derivative. Note that there is a significant difference between the characteristic frequencies for elastic waves, f_{el}, and heat conduction processes, f_{th}, in typical solids. Hence, the time-dependent thermal loadings under the frequency f_{th} do not give rise to elastic waves and elastic fields can be treated by the quasi-static approximation (with neglecting the inertia terms). Nevertheless, we consider this term in order to incorporate elastic waves into the simulations of the mechanical and the thermal processes under transient mechanical loadings. In

the case of thermal loadings including thermal shocks (sudden changes in thermal loading), one expects a vanishing influence of the inertia terms on the numerical results. On the other hand, the fast time-dependent mechanical loadings under the frequency f_{el} cannot be followed by the heat conduction and the adiabatic approximation takes place, i.e. there is no heat exchange between different places in the solids because of the absence of heat conduction. Then, the mechanical field is described by the elastodynamic theory with taking the adiabatic values of the material coefficients instead of the isothermal values. However, the coupling term in the heat conduction equation of coupled thermoelasticity is usually negligible and the thermal processes can be considered separately as independent on the mechanical field what is the assumption of the uncoupled thermoelasticity. Then, the multi-field problem is governed by the heat conduction equation and the equations of motion

$$[k_{ij}(\mathbf{x})\theta_{,j}(\mathbf{x},\tau)]_{,i} - \rho(\mathbf{x})c(\mathbf{x})\dot{\theta}(\mathbf{x},\tau) + Q(\mathbf{x},\tau) = 0, \tag{3}$$

$$\sigma_{ij,j}(\mathbf{x},\tau) + X_i(\mathbf{x},\tau) = \rho\ddot{u}_i(\mathbf{x},\tau), \tag{4}$$

where only the mechanical fields are affected by the thermal ones and $Q(\mathbf{x},\tau)$ is a body heat source.

A static problem can be considered formally as a special case of the dynamic one, by omitting the acceleration $\ddot{u}_i(\mathbf{x},\tau)$ in the equations of motion (4) and the time derivative term in equation (3). Therefore, both cases are analyzed in this paper simultaneously.

In the case of orthotropic materials, the relation between the stresses σ_{ij} and the strains ε_{ij} including the thermal expansion, is given by the well known Duhamel-Neumann constitutive equations for the stress tensor

$$\sigma_{ij}(\mathbf{x},\tau) = c_{ijkl}\varepsilon_{kl}(\mathbf{x},\tau) - \gamma_{ij}\theta(\mathbf{x},\tau), \tag{5}$$

where c_{ijkl} are the material's elastic constants and the stress-temperature moduli γ_{ij} can be expressed through the elastic constants and the linear thermal expansion coefficients α_{kl} as

$$\gamma_{ij} = c_{ijkl}\alpha_{kl}. \tag{6}$$

For 2-D plane problems, the constitutive equation (5) is frequently written in terms of the second-order tensor of the elastic constants [Lekhnitskii (1963)]. The constitutive equation for orthotropic materials and plane strain problems has the follow-

ing form

$$
\begin{bmatrix} \sigma_{11} \\ \sigma_{22} \\ \sigma_{12} \end{bmatrix} = \begin{bmatrix} c_{11} & c_{12} & 0 \\ c_{12} & c_{22} & 0 \\ 0 & 0 & c_{66} \end{bmatrix} \begin{bmatrix} \varepsilon_{11} \\ \varepsilon_{22} \\ 2\varepsilon_{12} \end{bmatrix} - \begin{bmatrix} c_{11} & c_{12} & c_{13} \\ c_{12} & c_{22} & c_{23} \\ 0 & 0 & 0 \end{bmatrix} \begin{bmatrix} \alpha_{11} \\ \alpha_{22} \\ \alpha_{33} \end{bmatrix} \theta
$$
$$
= \mathbf{C} \begin{bmatrix} \varepsilon_{11} \\ \varepsilon_{22} \\ 2\varepsilon_{12} \end{bmatrix} - \gamma\theta,
$$
(7)

with

$$
\gamma = \begin{bmatrix} c_{11} & c_{12} & c_{13} \\ c_{12} & c_{22} & c_{23} \\ 0 & 0 & 0 \end{bmatrix} \begin{bmatrix} \alpha_{11} \\ \alpha_{22} \\ \alpha_{33} \end{bmatrix} = \begin{bmatrix} \gamma_{11} \\ \gamma_{22} \\ 0 \end{bmatrix}.
$$

Equation (7) can be reduced to a simple form for isotropic materials

$$
\sigma_{ij} = 2\mu\varepsilon_{ij} + \lambda\varepsilon_{kk}\delta_{ij} - (3\lambda + 2\mu)\alpha\theta\delta_{ij}
$$
(8)

with Lame's constants λ and μ.

The following essential and natural boundary conditions are assumed for the mechanical quantities

$$
u_i(\mathbf{x}, \tau) = \tilde{u}_i(\mathbf{x}, \tau) \text{ on } \Gamma_u,
$$

$$
t_i(\mathbf{x}, \tau) = \sigma_{ij}(\mathbf{x}, \tau)n_j(\mathbf{x}) = \tilde{t}_i(\mathbf{x}, \tau) \text{ on } \Gamma_t,
$$

and for the thermal quantities

$$
\theta(\mathbf{x}, \tau) = \tilde{\theta}(\mathbf{x}, \tau) \text{ on } \Gamma_p,
$$

$$
q(\mathbf{x}, \tau) = k_{ij}\theta_{,j}(\mathbf{x}, \tau)n_i(\mathbf{x}) = \tilde{q}(\mathbf{x}, \tau) \text{ on } \Gamma_q,
$$

where Γ_u is the part of the global boundary with prescribed displacements, while on Γ_t, Γ_p and Γ_q the traction vector t_i, the temperature and the heat flux q are prescribed, respectively.

Initial conditions for the mechanical and thermal quantities are prescribed as

$$
u_i(\mathbf{x}, \tau)|_{\tau=0} = u_i(x, 0) \text{ and } \dot{u}_i(\mathbf{x}, \tau)|_{\tau=0} = \dot{u}_i(x, 0),
$$

$$
\theta(\mathbf{x}, \tau)|_{\tau=0} = \theta(x, 0) \text{ in } \Omega.
$$

The local weak-form of the governing equations (4) can be written as [Atluri, (2004), Sladek et al. (2006)]

$$\int\limits_{\Omega_s} \left[\sigma_{ij,j}(\mathbf{x}, \tau) - \rho \ddot{u}_i(\mathbf{x}, \tau) + X_i(\mathbf{x}, \tau)\right] u^*_{ik}(\mathbf{x}) \, d\Omega = 0, \tag{9}$$

where $u^*_{ik}(\mathbf{x})$ is a test function.

Applying the Gauss divergence theorem to the first integral results in

$$\int\limits_{\partial\Omega_s} \sigma_{ij}(\mathbf{x}, \tau) n_j(\mathbf{x}) u^*_{ik}(\mathbf{x}) d\Gamma - \int\limits_{\Omega_s} \sigma_{ij}(\mathbf{x}, \tau) u^*_{ik,j}(\mathbf{x}) d\Omega$$

$$+ \int\limits_{\Omega_s} \left[-\rho \ddot{u}_i(\mathbf{x}, \tau) + X_i(\mathbf{x}, \tau)\right] u^*_{ik}(\mathbf{x}) d\Omega = 0, \quad (10)$$

where $\partial\Omega_s$ is the boundary of the local subdomain which consists of three parts $\partial\Omega_s = L_s \cup \Gamma_{st} \cup \Gamma_{su}$ in general [Atluri, (2004)]. Here, L_s is the local boundary that is totally inside the global domain, Γ_{st} is the part of the local boundary which coincides with the global traction boundary, i.e., $\Gamma_{st} = \partial\Omega_s \cap \Gamma_t$, and similarly Γ_{su} is the part of the local boundary that coincides with the global displacement boundary, i.e., $\Gamma_{su} = \partial\Omega_s \cap \Gamma_u$.

By choosing a Heaviside step function as the test function $u^*_{ik}(\mathbf{x})$ in each subdomain

$$u^*_{ik}(\mathbf{x}) = \begin{cases} \delta_{ik} & \text{at } \mathbf{x} \in \Omega_s \\ 0 & \text{at } \mathbf{x} \notin \Omega_s \end{cases},$$

the local weak-form (10) is converted into the following local boundary-domain integral equations

$$\int\limits_{L_s+\Gamma_{su}} t_i(\mathbf{x}, \tau) d\Gamma - \int\limits_{\Omega_s} \rho \ddot{u}_i(\mathbf{x}, \tau) d\Omega = -\int\limits_{\Gamma_{st}} \tilde{t}_i(\mathbf{x}, \tau) d\Gamma - \int\limits_{\Omega_s} X_i(\mathbf{x}, \tau) d\Omega. \tag{11}$$

Equation (11) is recognized as the overall momentum equilibrium conditions on the subdomain Ω_s. Note that the local integral equations (LIEs) (11) are valid for both homogeneous and non-homogeneous solids. Non-homogeneous material properties are included in eq. (11) through the elastic constants and the thermo-elastic coefficients involved in the traction components

$$t_i(\mathbf{x}, \tau) = \left[c_{ijkl}(\mathbf{x}) u_{k,l}(\mathbf{x}, \tau) - \lambda_{ij}(\mathbf{x}) \theta(\mathbf{x}, \tau)\right] n_j(\mathbf{x}).$$

Similarly, the local weak-form of the governing equation (3) can be written as

$$\int_{\Omega_s} \left\{ [k_{ij}(\mathbf{x})\theta_{,j}(\mathbf{x},\tau)]_{,i} - \rho c \dot{\theta}(\mathbf{x},\tau) + Q(\mathbf{x},\tau) \right\} u^*(\mathbf{x})\, d\Omega = 0, \tag{12}$$

where $u^*(\mathbf{x})$ is a test function.

Applying the Gauss divergence theorem to the local weak-form and considering the Heaviside step function for the test function $u^*(\mathbf{x})$, one can obtain

$$\int_{L_s+\Gamma_{sp}} q(\mathbf{x},\tau)d\Gamma - \int_{\Omega_s} \rho c \dot{\theta}(x,\tau)d\Omega = -\int_{\Gamma_{sq}} \tilde{q}(\mathbf{x},\tau)d\Gamma - \int_{\Omega_s} Q(\mathbf{x},\tau)d\Omega. \tag{13}$$

Equation (13) is similarly recognized as the energy balance condition on the sub-domain.

3 Numerical solution procedure

In the MLPG method the test and the trial functions are not necessarily from the same functional spaces. For internal nodes, the test function is chosen as a unit step function with its support on the local subdomain. The trial functions, on the other hand, are chosen to be the MLS approximations by using a number of nodes spreading over the domain of influence. According to the MLS [Belytschko et al., (1996)] method, the approximation of the displacement field can be given as

$$\mathbf{u}^h(\mathbf{x}) = \sum_{i=1}^{m} p_i(\mathbf{x})a_i(\mathbf{x}) = \mathbf{p}^T(\mathbf{x})\mathbf{a}(\mathbf{x}), \tag{14}$$

where $\mathbf{p}^T(\mathbf{x}) = \{p_1(\mathbf{x}), p_2(\mathbf{x}), ...p_m(\mathbf{x})\}$ is a vector of complete basis functions of order m and $\mathbf{a}(\mathbf{x}) = \{a_1(\mathbf{x}), a_2(\mathbf{x}), ..., a_m(\mathbf{x})\}$ is a vector of unknown parameters that depend on $\mathbf{x}$. For example, in 2-D problems

$$\mathbf{p}^T(\mathbf{x}) = \{1, x_1, x_2\} \text{ for } m = 3$$

and

$$\mathbf{p}^T(\mathbf{x}) = \{1, x_1, x_2, x_1^2, x_1 x_2, x_2^2\} \text{ for } m = 6$$

are linear and quadratic basis functions, respectively. The basis functions are not necessary to be polynomials. It is convenient to introduce a $r^{-1/2}$ - singularity for

the secondary fields at the crack-tip vicinity for modelling crack problems [Fleming et al., (1997)]. Then, the basis functions can be taken as the following form

$$\mathbf{p}^T(\mathbf{x}) = \left\{ 1, x_1, x_3, \sqrt{r}\cos(\theta/2), \sqrt{r}\sin(\theta/2), \sqrt{r}\sin(\theta/2)\sin\theta, \sqrt{r}\cos(\theta/2)\sin\theta \right\}$$

$$\text{for } m = 7, \quad (15)$$

where r and θ are polar coordinates with the crack-tip as the origin.

The approximated functions for the mechanical displacements and the temperature can be written as [Atluri, (2004)]

$$\mathbf{u}^h(\mathbf{x},\tau) = \Phi^T(\mathbf{x}) \cdot \hat{\mathbf{u}} = \sum_{a=1}^{n} \phi^a(\mathbf{x})\hat{\mathbf{u}}^a(\tau), \quad (16)$$

$$\theta^h(\mathbf{x},\tau) = \sum_{a=1}^{n} \phi^a(\mathbf{x})\hat{\theta}^a(\tau), \quad (17)$$

where the nodal values $\hat{\mathbf{u}}^a(\tau) = (\hat{u}_1^a(\tau), \hat{u}_2^a(\tau))^T$, and $\hat{\theta}^a(\tau)$ are fictitious parameters for the displacements and the temperature, respectively, and $\phi^a(\mathbf{x})$ is the shape function associated with the node a. The number of nodes n used for the approximation is determined by the weight function $w^a(\mathbf{x})$. A 4th order spline-type weight function is applied in the present work

$$w^a(\mathbf{x}) = \begin{cases} 1 - 6\left(\frac{d^a}{r^a}\right)^2 + 8\left(\frac{d^a}{r^a}\right)^3 - 3\left(\frac{d^a}{r^a}\right)^4, & 0 \leq d^a \leq r^a \\ 0, & d^a \geq r^a \end{cases}, \quad (18)$$

where $d^a = \|\mathbf{x} - \mathbf{x}^a\|$ and r^a is the size of the support domain. The value of the radius of the support domain has been optimized on numerical experiments. Nie et al (2006) developed an efficient approach to find the optimal radius of support of radial weight functions used in MLS approximation.

It is seen that the C^1-continuity is ensured over the entire domain, and therefore the continuity conditions of the tractions and the heat flux are satisfied. However, this highly continuous nature leads to difficulties when there is an imposed discontinuity in the secondary fields (strains, gradients of the temperature). Because of the highly continuous trial function which is at least C^1, it is difficult to simulate jumps in the strain field. Krongauz and Belytschko (1998) introduced a jump shape function for 2-D problems. It is a trial function with a pre-imposed discontinuity in the gradient of the function at the location of the material discontinuity in addition to the MLS approximation. This method is very tedious for curvilinear interfaces. Cordes and Moran (1996) solved also 2-D problems by using Lagrangian multiplier. The method requires a lot of computational effort when the discontinuity is of an arbitrary geometrical shape.
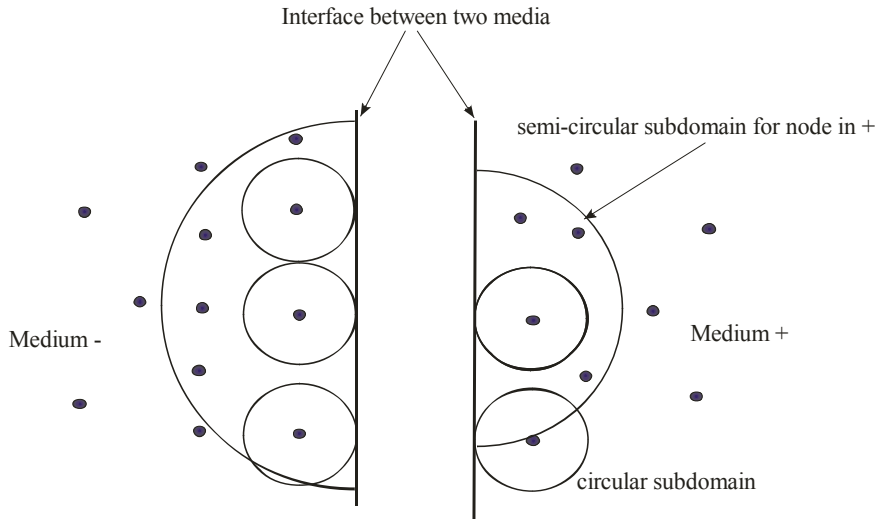
Figure 1: Modeling of material discontinuities

For 3-D problems it is much simpler to introduce double nodes in the material discontinuity [Li et al. (2003)]. Two sets of collocation nodes are assigned on both the +side and the –side of the material interface at the same location, but with different material properties (Fig. 1). The MLS approximations are carried out separately on particular sets of nodes within each of the homogeneous domains. Then, the support domains for the weights in the weighted MLS-approximations are truncated at the interface of the two media. Therefore, the high order continuity is kept within each homogeneous part, but not across their interface. Also the local subdomains considered around nodes should not cross the interface.

The traction vectors $t_i(\mathbf{x}, \tau)$ at a boundary point $\mathbf{x} \in \partial\Omega_s$ are approximated in terms of the same nodal values $\hat{\mathbf{u}}^a(\tau)$ and $\hat{\theta}^a(\tau)$ as

$$\mathbf{t}^h(\mathbf{x}, \tau) = \mathbf{N}(\mathbf{x})\mathbf{C}\sum_{a=1}^{n}\mathbf{B}^a(\mathbf{x})\hat{\mathbf{u}}^a(\tau) - \mathbf{N}(\mathbf{x})\gamma\sum_{a=1}^{n}\phi^a(\mathbf{x})\hat{\theta}^a(\tau), \qquad (19)$$

where the matrix $\mathbf{N}(\mathbf{x})$ is related to the normal vector $\mathbf{n}(\mathbf{x})$ on $\partial\Omega_s$ by

$$\mathbf{N}(\mathbf{x}) = \begin{bmatrix} n_1 & 0 & n_2 \\ 0 & n_2 & n_1 \end{bmatrix}.$$

The matrix $\mathbf{B}^a$ is represented by the gradients of the shape functions

$$\mathbf{B}^a(\mathbf{x}) = \begin{bmatrix} \phi_{,1}^a & 0 \\ 0 & \phi_{,2}^a \\ \phi_{,2}^a & \phi_{,1}^a \end{bmatrix}.$$

Similarly the heat flux $q(\mathbf{x}, \tau)$ can be approximated by

$$q^h(\mathbf{x}, \tau) = k_{ij} n_i \sum_{a=1}^{n} \phi_{,j}^a(\mathbf{x}) \hat{\theta}^a(\tau) = \mathbf{n}^T(\mathbf{x}) \mathbf{K}(\mathbf{x}) \sum_{a=1}^{n} \mathbf{P}^a(\mathbf{x}) \hat{\theta}^a(\tau), \tag{20}$$

where

$$\mathbf{K}(\mathbf{x}) = \begin{bmatrix} k_{11} & k_{12} \\ k_{21} & k_{22} \end{bmatrix}, \quad \mathbf{P}^a(\mathbf{x}) = \begin{bmatrix} \phi_{,1}^a \\ \phi_{,2}^a \end{bmatrix}, \quad \mathbf{n}^T(\mathbf{x}) = (n_1, n_2).$$

The local integral equation for the heat conduction, eq. (13), considered at each interior point $\mathbf{x}^i \in \Omega_s^i \subset \Omega$, yields the following set of equations

$$\sum_{a=1}^{n} \hat{\theta}^a(\tau) \int_{\partial \Omega_s^i} \mathbf{n}^T(\mathbf{x}) \mathbf{K}(\mathbf{x}) \mathbf{P}^a(\mathbf{x}) d\Gamma - \sum_{a=1}^{n} \dot{\hat{\theta}}^a(\tau) \int_{\Omega_s^i} \rho c \phi^a(\mathbf{x}) d\Omega = - \int_{\Omega_s^i} Q(\mathbf{x}, \tau) d\Omega. \tag{21}$$

Substituting the MLS approximations for the displacements (16) and the tractions (19) into (11) for each interior node $\mathbf{x}^i$, the following set of discretized LIEs for the mechanical field is obtained

$$\sum_{a=1}^{n} \left[\left(\int_{L_s^i} \mathbf{N}(\mathbf{x}) \mathbf{C} \mathbf{B}^a(\mathbf{x}) d\Gamma \right) \hat{\mathbf{u}}^a(\tau) - \rho \left(\int_{\Omega_s^i} \phi^a(\mathbf{x}) d\Omega \right) \ddot{\hat{\mathbf{u}}}^a(\tau) \right] -$$

$$- \sum_{a=1}^{n} \left(\int_{L_s + \Gamma_{su}} \mathbf{N}(\mathbf{x}) \gamma \phi^a(\mathbf{x}) d\Gamma \right) \hat{\theta}^a(\tau) =$$

$$= - \int_{\Omega_s^i} \mathbf{X}(\mathbf{x}, \tau) d\Omega. \tag{22}$$

The discretized displacement, traction, temperature and heat flux boundary conditions

$$\sum_{a=1}^{n} \phi^a(\mathbf{x}^b) \hat{\mathbf{u}}^a(\tau) = \tilde{\mathbf{u}}(\mathbf{x}^b, \tau) \text{ for } \mathbf{x}^b \in \partial \Omega_s^b \cap \Gamma_u = \Gamma_{su}^b, \tag{23}$$

$$\mathbf{N}(\mathbf{x}^b)\left[\mathbf{C}\sum_{a=1}^{n}\mathbf{B}^a(\mathbf{x}^b)\hat{\mathbf{u}}^a(\tau) - \gamma\sum_{a=1}^{n}\phi^a(\mathbf{x}^b)\hat{\theta}^a(\tau)\right] = \tilde{\mathbf{t}}(\mathbf{x}^b,\tau) \text{ for } \mathbf{x}^b \in \partial\Omega_s^b \cap \Gamma_t = \Gamma_{st}^b,$$

$$(24)$$

$$\sum_{a=1}^{n}\phi^a(\mathbf{x}^b)\hat{\theta}^a(\tau) = \tilde{\theta}(\mathbf{x}^b,\tau) \text{ for } \mathbf{x}^b \in \partial\Omega_s^b \cap \Gamma_p = \Gamma_{sp}^b, \qquad (25)$$

$$\mathbf{n}^T(\mathbf{x}^b)\mathbf{K}(\mathbf{x}^b)\sum_{a=1}^{n}\mathbf{P}^a(\mathbf{x}^b)\hat{\theta}^a(\tau) = \tilde{q}(\mathbf{x}^b,\tau) \text{ for } \mathbf{x}^b \in \partial\Omega_s^b \cap \Gamma_q = \Gamma_{sq}^b \qquad (26)$$

are considered at boundary nodes $\mathbf{x}^b \in \Gamma = \Gamma_u \cup \Gamma_t \cup \Gamma_p \cup \Gamma_q$.

On the interface Γ_I of the two material media there are no boundary conditions prescribed but we can guarantee the continuity for the displacements and the temperature, as well as the equilibrium for tractions and heat flux by collocating the following equations at double nodes $\mathbf{x}^d \in \partial\Omega_s^d \cap \Gamma_I = \Gamma_I^d$

$$\sum_{a=1}^{n^+}\phi^a(\mathbf{x}^d)\hat{\mathbf{u}}^a(\tau) = \sum_{a=1}^{n^-}\phi^a(\mathbf{x}^d)\hat{\mathbf{u}}^a(\tau),$$

$$\sum_{a=1}^{n^+}\phi^a(\mathbf{x}^d)\hat{\theta}^a(\tau) = \sum_{a=1}^{n^-}\phi^a(\mathbf{x}^d)\hat{\theta}^a(\tau),$$

$$\mathbf{N}(\mathbf{x}^d)\left[\mathbf{C}^+(\mathbf{x}^d)\sum_{a=1}^{n^+}\mathbf{B}^a(\mathbf{x}^d)\hat{\mathbf{u}}^a(\tau) - \gamma^+(\mathbf{x}^d)\sum_{a=1}^{n^+}\phi^a(\mathbf{x}^d)\hat{\theta}^a(\tau) - \right.$$

$$\left. - \mathbf{C}^-(\mathbf{x}^d)\sum_{a=1}^{n^-}\mathbf{B}^a(\mathbf{x}^d)\hat{\mathbf{u}}^a(\tau) + \gamma^-(\mathbf{x}^d)\sum_{a=1}^{n^-}\phi^a(\mathbf{x}^d)\hat{\theta}^a(\tau)\right] = 0,$$

$$\mathbf{n}^T(\mathbf{x}^d)\left[\mathbf{K}^+(\mathbf{x}^d)\sum_{a=1}^{n^+}\mathbf{P}^a(\mathbf{x}^d)\hat{\theta}^a(\tau) - \mathbf{K}^-(\mathbf{x}^d)\sum_{a=1}^{n^-}\mathbf{P}^a(\mathbf{x}^d)\hat{\theta}^a(\tau)\right] = 0, \qquad (27)$$

where n^+ and n^- are the numbers of nodes lying in the support domain in medium + and medium -, respectively. The normal vector components in $\mathbf{N}(\mathbf{x}^d)$ and $\mathbf{n}^T(\mathbf{x}^d)$ are taken in the sense of outward normal to the medium +.

The backward finite difference method is applied to the approximation of "velocities"

$$\dot{\mathbf{y}}_{\tau+\Delta\tau} = \frac{\mathbf{y}_{\tau+\Delta\tau} - \mathbf{y}_\tau}{\Delta\tau}, \qquad (28)$$

where $\Delta\tau$ is the time-step.

The system of ordinary differential equations (21) and collocation equations (25)-(27) can be rearranged in such a way that all known quantities are in the second term of the matrix form the system equations, viz.

$$\mathbf{A}\dot{\mathbf{y}} + \mathbf{B}\mathbf{y} = \mathbf{Q}. \tag{29}$$

Substituting eq. (28) into eq. (29) results in the following set of algebraic equations for the unknowns $\mathbf{y}_{\tau+\Delta\tau}$

$$\left[\frac{1}{\Delta\tau}\mathbf{A} + \mathbf{B}\right]\mathbf{y}_{\tau+\Delta\tau} = \mathbf{A}\frac{1}{\Delta\tau}\{\mathbf{y}_\tau\} + \mathbf{Q}. \tag{30}$$

Once the temperature field is computed from eq. (30), the mechanical field can be determined. The matrix form of the ordinary differential equations (22) and the collocation equations (23), (24) and (27) can be written as

$$\mathbf{L}\ddot{\mathbf{x}} + \mathbf{K}\mathbf{x} = \mathbf{P}. \tag{31}$$

Several time integration procedures for the solution of this system of ordinary differential equations are available. In the present work, the Houbolt finite difference scheme [Houbolt (1950)] is adopted in which the acceleration $\ddot{\mathbf{u}} = \ddot{\mathbf{x}}$ is expressed as

$$\ddot{\mathbf{x}}_{\tau+\Delta\tau} = \frac{2\mathbf{x}_{\tau+\Delta\tau} - 5\mathbf{x}_\tau + 4\mathbf{x}_{\tau-\Delta\tau} - \mathbf{x}_{\tau-2\Delta\tau}}{\Delta\tau^2}, \tag{32}$$

where $\Delta\tau$ is the time-step.

Substituting eq. (32) into eq. (31), the following system of algebraic equations is obtained for the unknowns $\mathbf{x}_{\tau+\Delta\tau}$

$$\left[\frac{2}{\Delta\tau^2}\mathbf{L} + \mathbf{K}\right]x_{\tau+\Delta\tau} = \mathbf{L}\frac{1}{\Delta\tau^2}\{5\mathbf{x}_\tau - 4\mathbf{x}_{\tau-\Delta\tau} + \mathbf{x}_{\tau-2\Delta\tau}\} + \mathbf{P}. \tag{33}$$

To ensure the stability, the value of the time-step has to be appropriately selected with respect to the material parameters (elastic wave velocities) and the time dependence of the boundary conditions.

4 Evaluation of stress intensity factors

For crack-tips inside a homogeneous anisotropic solid there is a well-known $\sqrt{r}$-behaviour for the displacements at the crack-tip vicinity. This allows us to compute

the stress intensity factors (SIFs) from the asymptotic expansion of the displacements by an extrapolation technique. Both mode-I and mode-II SIFs can be computed from the following equations [Zhang (2005)]

$$
\begin{Bmatrix} K_{II}(\tau) \\ K_I(\tau) \end{Bmatrix} = \frac{1}{4\Delta}\sqrt{\frac{2\pi}{l}} \begin{bmatrix} H_{11} & H_{12} \\ H_{21} & H_{22} \end{bmatrix} \begin{Bmatrix} \Delta u_1(l,\tau) \\ \Delta u_2(l,\tau) \end{Bmatrix}, \tag{34}
$$

where l is a distance from the point evaluating the crack-opening-displacements Δu_i to the crack-tip and

$$
\begin{bmatrix} H_{11} & H_{12} \\ H_{21} & H_{22} \end{bmatrix} = \begin{bmatrix} Im\left(\frac{q_1-q_2}{\mu_1-\mu_2}\right) & Im\left(\frac{p_2-p_1}{\mu_1-\mu_2}\right) \\ Im\left(\frac{\mu_1 q_2-\mu_2 q_1}{\mu_1-\mu_2}\right) & Im\left(\frac{\mu_2 q_1-\mu_1 q_2}{\mu_1-\mu_2}\right) \end{bmatrix}, \tag{35}
$$

$\Delta = H_{11}H_{22} - H_{12}H_{21}$.

In equations (35) μ_α denotes the complex roots of the characteristic equation [Lekhnitskii (1963)]

$$
b_{11}\mu_\alpha^4 - 2b_{16}\mu_\alpha^3 + (2b_{12}+b_{66})\mu_\alpha^2 - 2b_{26}\mu_\alpha + b_{22} = 0, \tag{36}
$$

with b_{ij} being the material compliances and

$$
p_\alpha = b_{11}\mu_\alpha^2 - b_{16}\mu_\alpha + b_{12},
$$

$$
q_\alpha = (b_{12}\mu_\alpha^2 - b_{26}\mu_\alpha + b_{22})/\mu_\alpha.
$$

For interface cracks between dissimilar anisotropic materials, the displacements at the crack-tip vicinity show an oscillating behaviour $\sqrt{r}\cos(\varepsilon \ln r)$, where ε is the bi-material constant which describes the mismatch of the elastic properties. The absolute value of the stress intensity factor $|K|$ and the phase angle ϕ of the complex SIF are defined by Cho et al. (1992)

$$
|K(\tau)| = \sqrt{K_1^2 + K_2^2} = \frac{1+4\varepsilon^2}{4\cosh\pi\varepsilon}\sqrt{\frac{2\pi}{l}}\frac{\sqrt{t_{21}^2+d_{21}^2}}{d_1 t_2 - t_1 d_2}, \tag{37}
$$

$$
\tan\phi(\tau) = \frac{K_2(\tau)}{K_1(\tau)} = \frac{d_2 - d_1\left[\Delta u_2(l,\tau)/\Delta u_1(l,\tau)\right]}{t_1\left[\Delta u_2(l,\tau)/\Delta u_1(l,\tau)\right] - t_2}, \tag{38}
$$

where

$$
t_{21} = t_2\Delta u_1(l,\tau) - t_1\Delta u_2(l,\tau),
$$

$d_{21} = d_1 \Delta u_2(l, \tau) - d_2 \Delta u_1(l, \tau).$

The constants d_α, t_α and the bi-material constant ε are defined in Appendix [Wünsche et al. (2009)]. An extrapolation technique is applied to the above given equations and the crack-opening displacements are computed at three different nodes on the crack-faces. Indeed, the oscillatory stress singularity at the crack-tips can be taken into account in the shape-functions in a refined approach as presented by Tan et al. (1992) and Ang et al. (1996).

5 Numerical examples

5.1 *A central crack in a finite plate under a pure mechanical load*

In the first example a straight central crack in a finite plate under a pure mechanical load is analyzed. The central crack with length 2a is considered on the interface of two dissimilar anisotropic materials (Fig. 2). The rectangular plate is subjected to a tensile load at the top and bottom part of the plate. The following geometrical values are considered in the numerical analysis: $a = 0.5m$, width ratio of the plate $a/w = 0.4$ and height ratio $h/w = 1.2$.
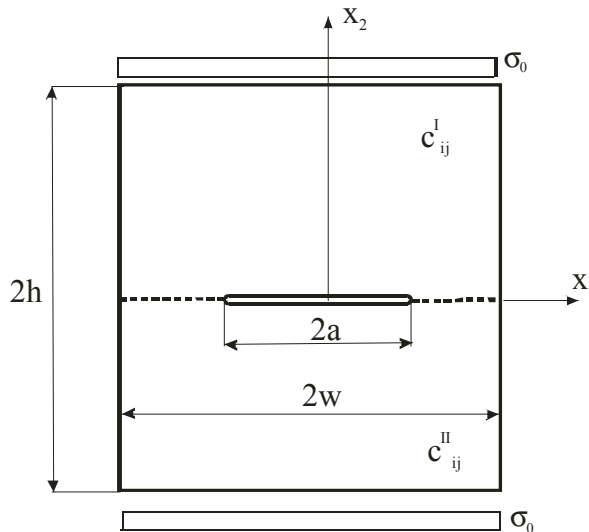
Figure 2: A central interface crack in a layered rectangular plate

To test the accuracy of the present computational method we have analyzed a crack in a homogeneous anisotropic plate corresponding to a graphite-epoxy composite with a composition of 65% graphite and 35% epoxy and the following elastic

stiffness matrix

$$
\begin{bmatrix}
155.43 & 3.72 & 3.72 & 0 & 0 & 0 \\
 & 16.34 & 4.96 & 0 & 0 & 0 \\
 & & 16.34 & 0 & 0 & 0 \\
 & & & 3.37 & 0 & 0 \\
 & \textit{sym.} & & & 7.48 & 0 \\
 & & & & & 7.48
\end{bmatrix} \cdot 10^9 N/m^2 .
$$

A static tensile load $\sigma_0 = 1Pa$ and plane strain conditions are considered. Due to the symmetry of the problem with respect to x_2-axis, only a half of the strip is modeled. We have used 1860 (2x31x30) nodes equidistantly distributed for the MLS approximation of the physical quantities (Fig. 3). The symmetry with respect to the x_1-axis is not utilized owing to test the computational scheme for further calculations of piece-wise homogeneous media. The local subdomains are considered to be circular with a radius $r_{loc} = 0.033m$.
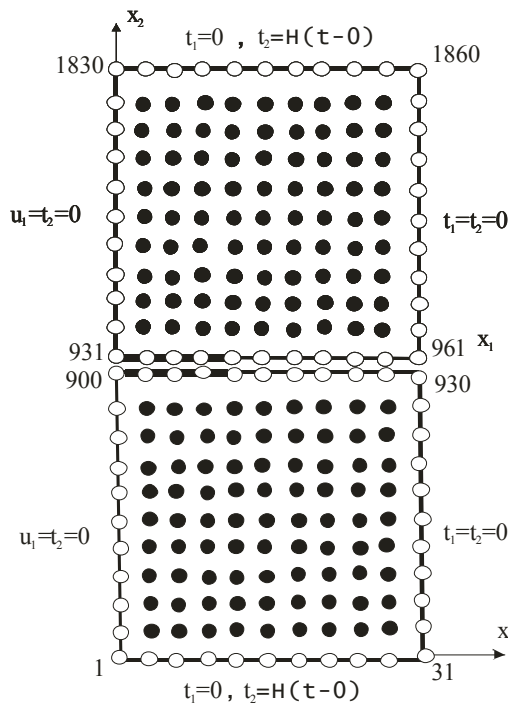
Figure 3: Node distribution and boundary conditions

The crack-displacements on both crack-faces are presented in Fig. 4. One can

observe a good agreement between the MLPG and the FEM results obtained by ANSYS computer code with PLANE 183 elements. The corresponding normalized mode-I SIF $K_I/\sigma_0\sqrt{\pi a} = 1.108$ is also in a good agreement with the reference value of the handbook [Murakami (1987)]
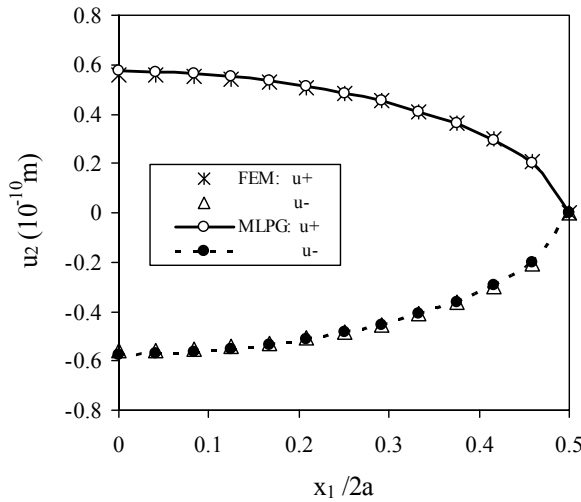

Figure 4: Variations of the crack-displacements with the normalized coordinate $x_1/2a$ in a homogeneous anisotropic plate subjected to a static tension

Now, we consider an inhomogeneous plate with isotropic material properties in the upper part I with Young's modulus $E = 100Mpa$ and Poisson's ratio $v = 0.3$, and orthotropic properties in the lower part II with $E_1 = E_3 = 1 \cdot 10^{11} N/m^2, E_2 = 3 \cdot 10^{11} N/m^2$, shear moduli $G_{12} = G_{23} = 38.46 \cdot 10^9 N/m^2$, $G_{13} = 115.4 \cdot 10^9 N/m^2$ and Poisson's ratios $v_{12} = v_{32} = 0.1$ and $v_{21} = v_{23} = v_{13} = 0.3$. The corresponding elastic stiffness matrix for the orthotropic material can be obtained by the inversion of the compliance matrix as follows

$$
\begin{bmatrix}
116.6 & 46.88 & 39.66 & 0 & 0 & 0 \\
 & 328.1 & 46.88 & 0 & 0 & 0 \\
 & & 116.6 & 0 & 0 & 0 \\
 & & & 38.46 & 0 & 0 \\
 & sym. & & & 115.4 & 0 \\
 & & & & & 38.46
\end{bmatrix} \cdot 10^9 N/m^2 .
$$

The crack-displacements on both crack-faces in the inhomogeneous plate subjected

to a static tension are presented in Fig. 5. The displacement on the lower crack-face u_2^- in the inhomogeneous interface crack problem is significantly reduced with respect to the homogeneous case. It is due to the larger stiffness coefficient c_{22} corresponding to a Young's moduli relation $E_2 = 3E_1$. The interface crack problem
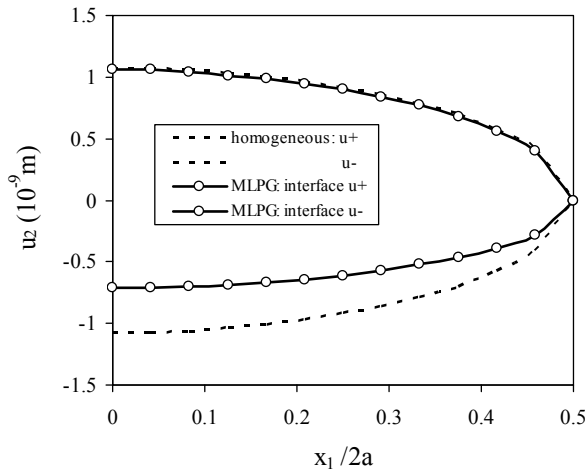

Figure 5: Variations of the crack-displacements with the normalized coordinate $x_1/2a$ for a static tension

has been analyzed also by FEM. The numerical results for the displacement u_2 are compared in Fig. 6 and a good agreement can be observed for both crack-faces.

The same interface crack problem under an impact load with Heaviside time variation is analyzed too. The mass density corresponds to graphite-epoxy composite with $\rho = 2000 kgm^{-3}$ and the same material and geometrical parameters are used for the upper and lower parts of the specimen. The number of nodes for MLS approximations is the same as in the static case and a time-step of $\Delta t = 7\mu s$ is chosen.

The time variation of the normalized absolute value of SIF, $|K(t)|/\sigma_0\sqrt{\pi a}$, is presented in Fig. 7, where the FEM, BEM and MLPG results are compared. One can observe a very good agreement of the numerical results.

5.2 A central crack in a finite plate under a thermal load

The geometry of the strip is given in Fig. 8 with the following values: $a = 0.5$, $a/w = 0.4$ and $h/w = 1.2$. On the outer boundary of the strip a thermal load $T_2 =$
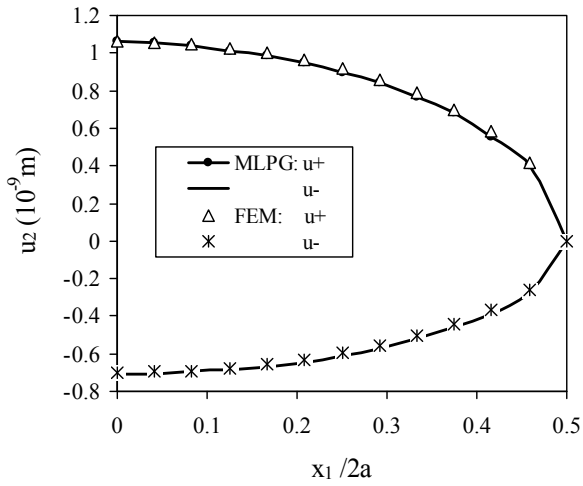
Figure 6: Variations of the crack-displacements with the normalized coordinate $x_1/2a$ for a static tension
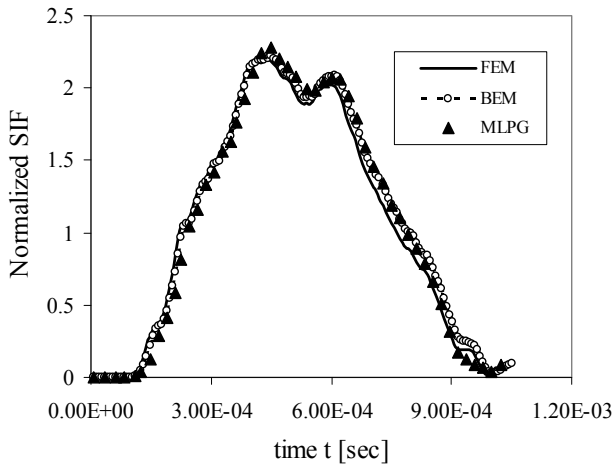

Figure 7: Time variation of the normalized absolute value of SIF

$\theta_0 = 1\,\text{deg}$ is applied. On both crack-faces a vanishing temperature is kept $T_1 = 0$. The outer boundary is free of tractions.

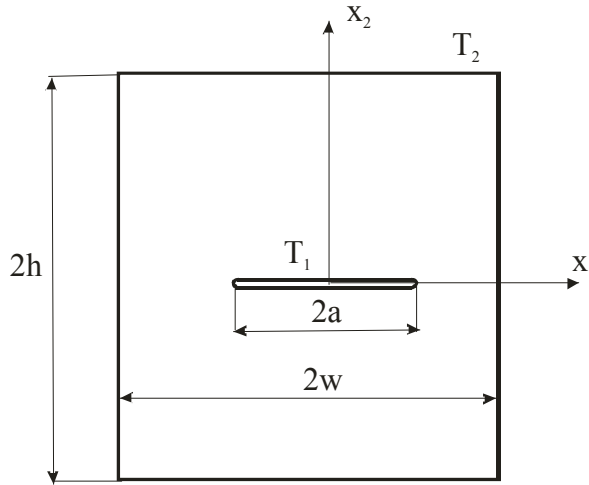Due to the symmetry of the problem with respect to x_2-axis, again only a half

Figure 8: Central crack in a finite plate with prescribed temperatures on outer boundary and crack-faces

of the strip is modeled. We have used 1860 (2x31x30) nodes equidistantly distributed for the MLS approximation of the physical quantities (Fig. 9). The local subdomains are considered to be circular with a radius $r_{loc} = 0.033m$. Homogeneous material properties are selected to test the present computational method. The material constants correspond to an isotropic material with Young's modulus $E = 100MPa$, Poisson's ratio $v = 0.3$, mass density $\rho = 7500kg/m^3$, thermal conductivity $k = 75\,W/Km$, thermal expansion $\alpha = 0.4 \cdot 10^{-5}1/K$ and specific heat conduction $c = 420Wskg^{-1}K^{-1}$. Numerical results obtained by FEM and the present MLPG are compared in Fig. 10. The stress intensity factor for this case is equal to $K_I^{stat}(\text{hom.}) = 2.02 \cdot 10^5 Pam^{1/2}$. One can observe a very good agreement of the MLPG and the FEM results. After the numerical test of the accuracy we consider now the interface crack problem, where isotropic material properties in the upper part I with Young's modulus $E = 100MPa$ and Poisson's ratio $v = 0.3$, and orthotropic properties in the lower part II with $E_1 = E_3 = 1 \cdot 10^{11}N/m^2$, $E_2 = 3 \cdot 10^{11}N/m^2$, shear moduli $G_{12} = G_{23} = 38.46 \cdot 10^9N/m^2$ and $G_{13} = 115.4 \cdot 10^9N/m^2$ and Poisson's ratios $v_{12} = v_{32} = 0.1$ and $v_{21} = v_{23} = v_{13} = 0.3$ are considered. The thermal conductivity $k = 75\,W/Km$, thermal expansion $\alpha = 0.4 \cdot 10^{-5}1/K$ and specific heat conduction $c = 420Wskg^{-1}K^{-1}$ are used for the upper part I and orthotropic properties $k_{11} = 150W/Km$, $k_{22} = 100W/Km$, $k_{12} = 0$, $\alpha_{11} = 0.8 \cdot 10^{-5}1/K$, $\alpha_{22} = \alpha_{33} = 0.4 \cdot 10^{-5}1/K$ for part II. The variations of the crack-opening-displacement Δu_2 along the x_1-coordinate on the crack-faces

are presented in Fig. 10 for homogeneous and dissimilar materials. One can see that the crack-opening-displacement is slightly higher for the interface crack between two dissimilar materials than for the crack in a homogeneous material. One can again observe a very good agreement of the FEM and the MLPG results.
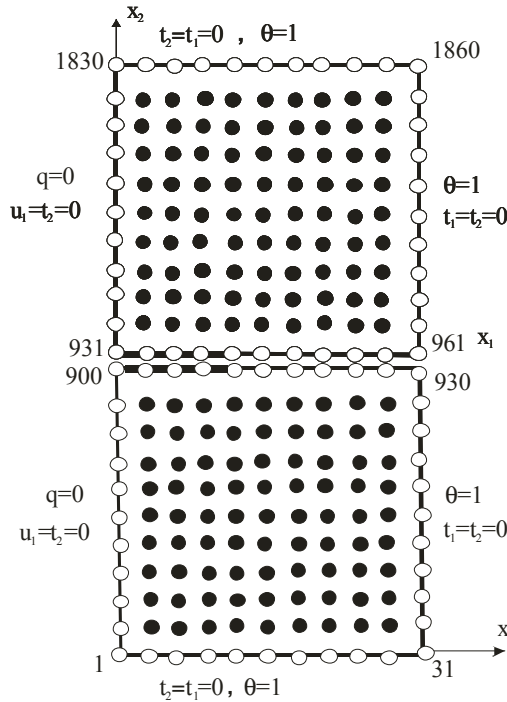

Figure 9: Node distribution and boundary conditions

The stress intensity factor for an interface crack between two dissimilar orthotropic materials is a little bit higher than that one in a homogeneous material, $K_I^{stat}(\mathrm{non}-\mathrm{hom.}) = 2.12 \cdot 10^5 Pa\,m^{1/2}$. Figure 11 presents the variation of the temperature ahead the crack-tip at $x_2 = 0$. The temperature variations are almost the same for a crack in a homogeneous material and an interface crack between two dissimilar materials. A slight difference between the temperature variations along x_2 at $x_1/2a = 0.5$ is observed on Fig. 12. Higher temperature values occur in the lower part of the inhomogeneous plate, where larger thermal conductivity values are considered than in the upper part or in the homogeneous case.

Finally, we consider a thermal shock on the outer boundary of the finite plate with a central crack. Heaviside time variation is taken for the thermal shock. The material properties are the same as in the previous static case. Now, we choose the
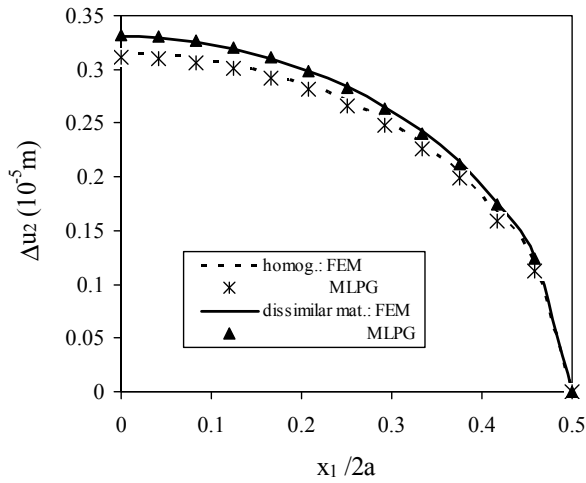
Figure 10: Variations of the crack-opening-displacement with the normalized co-ordinate $x_1/2a$ in a plate subjected to a stationary thermal load
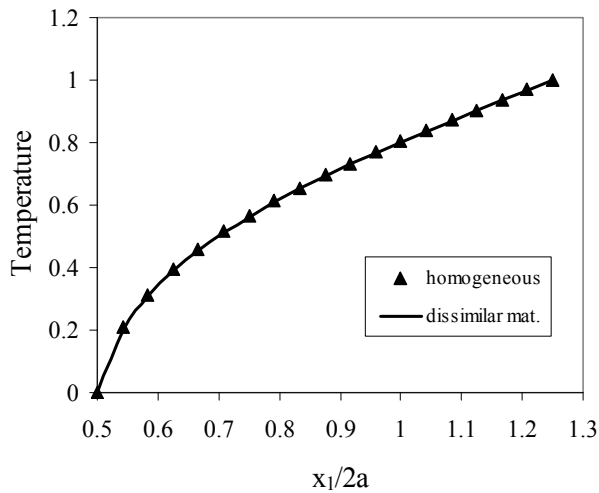

Figure 11: Variations of the temperature ahead the crack-tip in a plate subjected to a stationary thermal load
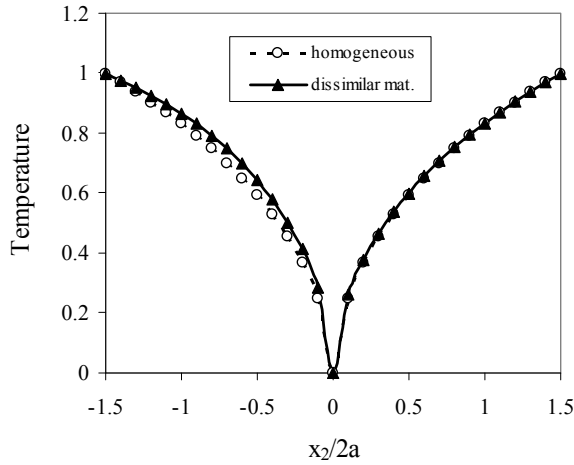
Figure 12: Variations of the temperature along x_2 at $x_1/2a = 0.5$ in a plate subjected to a stationary thermal load

mass density as $\rho = 7500 kg/m^3$. The time variation of the temperature ahead the crack-tip at two different nodes is presented in Fig. 13 for a homogeneous material. The time-step appropriate for the evolution of the thermal field has been selected as $\Delta t = 250s$. The stress intensity factor is normalized by the static value with homogeneous material properties, $K_I^{stat}(\text{hom.}) = 2.02 \cdot 10^5 Pa m^{1/2}$. One can see in Fig. 14, that the maximum stress intensity factor is reached in infinite time for a homogeneous plate, when the maximum temperature gradient occurs. However, for an interface crack between two dissimilar materials the maximum temperature gradient is reached in a finite instant and therefore the maximum stress intensity factor is observed just at that time. Then, the stress intensity factor is slowly decreasing to the static value $K_I^{stat}(\text{non - hom.}) = 2.12 \cdot 10^5 Pa m^{1/2}$.

From the comparison of Figs. 7 and 14, one can see the difference in the time variations of the SIFs corresponding to the transient mechanical and transient thermal loads. Furthermore, the times needed for reaching the maximum values of the SIF differ in 7 orders, caused by the difference in the characteristic frequencies for the mechanical and the thermal processes. The time evolution of the elastic field follows that of the thermal field in the case of thermal loading. Then, the consideration of the acceleration term according to eq. (32) with a large time-step (adequate for time variations induced by the thermal loading) results in a negligible inertial term **Lẍ** in eq. (31). Thus, the influence of the inertial term is negligible and the mechanical field can be described by the quasi-static approximation even in the case
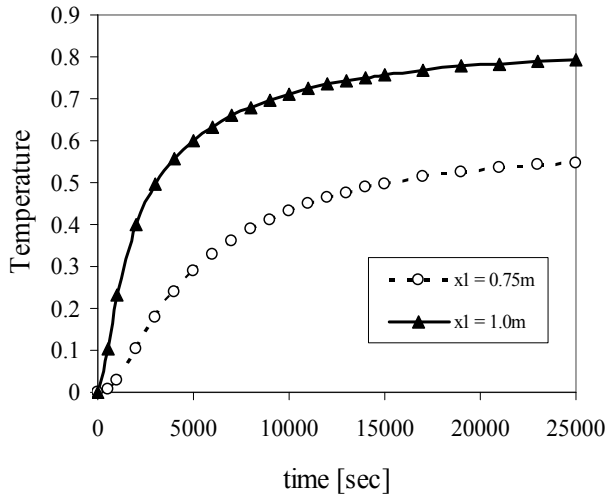
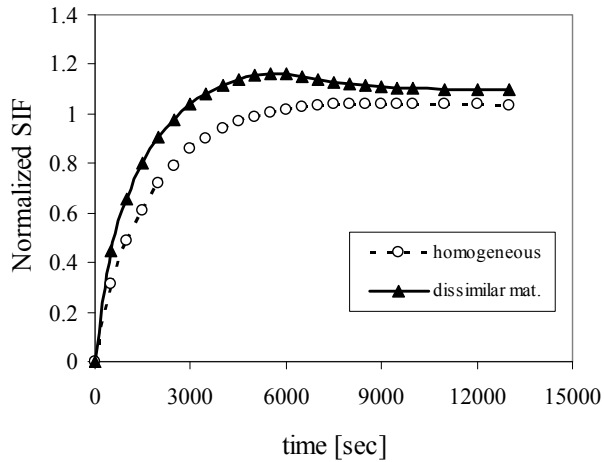Figure 13: Time variations of the temperature ahead the crack-tip at two different nodes

Figure 14: Time variations of the SIF for a crack in a homogeneous material and an interface crack between two dissimilar materials

of a thermal shock loading, since the time variation of the temperature field is very slow in comparison with that of elastic waves.

6   Conclusions

A meshless local Petrov-Galerkin method (MLPG) is presented for 2-D interface crack problems between two dissimilar anisotropic materials. Both mechanical and thermal loads at stationary (static) and transient conditions are considered here. The governing partial differential equations are satisfied in a weak-form on small fictitious subdomains. A unit step function is used as the test function in the local weak-form of the governing partial differential equations on small circular subdomains spread on the analyzed domain. The moving least-squares (MLS) scheme is adopted for the approximation of the physical field quantities. One obtains a system of ordinary differential equations for certain nodal unknowns. The backward finite difference method is applied for the approximation of the diffusive term in the heat conduction equation. Then, the system of the ordinary differential equations of the second order resulting from the equations of motion is solved by the Houbolt finite-difference scheme as a time-stepping method. The proposed method is a truly meshless method, which requires neither domain elements nor background cells in either the interpolation or the integration.

The present method is an alternative numerical tool to many existing computational methods such as the FEM or the BEM. The main advantage of the present method is its simplicity. Compared to the conventional BEM, the present method requires no fundamental solutions and all integrands in the present formulation are regular. Thus, no special numerical techniques are required to evaluate the integrals. It should be noted here that the expressions of the fundamental solutions for anisotropic materials in transient elastodynamics are quite complicated and their usage may not be efficient. The present formulation also possesses the generality of the FEM. Therefore, the method is promising for numerical analysis of multi-field problems.

References

Ang, H.E.; Torrance, J.E.; Tan, C.L. (1996): Boundary element analysis of orthotropic delamination specimen with interface cracks. *Engn. Fracture Mechanics*,

54: 601-615.

Atkinson, C. (1977): On stress singularities and interfaces in linear elastic fracture mechanics. *Int. Journal of Fracture,* 13: 807-820.

Atluri, S.N. (2004): *The Meshless Method,* **(MLPG) for Domain & BIE Discretizations**. Tech Science Press.

Atluri, S.N.; Zhu, T. (1998): A new Meshless Local Petrov-Galerkin (MLPG) approach in computational mechanics. *Computational Mechanics*, 22: 117-127.

Atluri, S.N.; Sladek, J.; Sladek, V.; Zhu, T. (2000): The local boundary integral equation (LBIE) and its meshless implementation for linear elasticity. *Computational Mechanics*, 25: 180-198.

Atluri, S.N.; Han, Z.D.; Shen, S. (2003): Meshless local Petrov-Galerkin (MLPG) approaches for solving the weakly-singular traction & displacement boundary integral equations. *CMES: Computer Modeling in Engineering & Sciences*, 4: 507-516.

Batra, R.C.; Porfiri, M.; Spinello, D. (2004): Treatment of material discontinuity in two Meshless local Petrov-Galerkin (MLPG) formulations of axisymmetric transient heat conduction. *Int. J. Num. Meth. Engn.*, 61: 2461-2479.

Belytschko, T.; Krogauz, Y.; Organ, D.; Fleming, M.; Krysl, P. (1996): Meshless methods; an overview and recent developments. *Computer Methods in Applied Mechanics and Engineering,* 139: 3-47.

Bobaru, F.; Mukherjee, S. (2003): Meshless approach to shape optimization of linear thermoelastic solids. *Int. J. Num. Meth. Engn.*, 53: 765-796.

Chen, J.; Dargush, G.F. (1995): Boundary element method for dynamic poroelastic and thermoelastic analyses. *Int. J. Solids and Structures*, 32: 2257-2278.

Cho, S.B.; Lee, K.B.; Choy, Y.S.; Yuuki, R. (1992): Determination of stress intensity factors and boundary element analysis for interface cracks in dissimilar anisotropic materials. *Engn. Fracture Mechanics*, 43: 603-614.

Comninou, M. (1977): The interfacial crack. *ASME Journal of Applied Mechanics*, 44: 631-636 .

Comninou, M.; Schmeser, D. (1979): The interfacial crack in a combined tension-compression and shear field. *ASME Journal of Applied Mechanics,* 46: 345-348.

Cordes, L.W.; Moran, B. (1996): Treatment of material discontinuity in the element free Galerkin method. *Comput. Meth. Appl. Mech. Engn.*, 139: 75-89.

Dargush, G.F.; Banerjee, P.K. (1991): A new boundary element method for three-dimensional coupled problems of conduction and thermoelasticity. *ASME J. Appl. Mech.*, 58: 28-36.

England, A.H. (1965): A crack between dissimilar media. *ASME Journal of Applied Mechanics*, 32: 400-402.

Erdogan, F. (1963): Stress distribution in a nonhomogeneous elastic plane with cracks. *ASME Journal of Applied Mechanics*, 30: 232-236.

Erdogan, F. (1965): Stress distribution in bonded dissimilar materials with cracks. *ASME Journal of Applied Mechanics*, 32: 403-410.

Fleming, M.; Chu, Y.A.; Moran, B.; Belytschko, T. (1997): Enriched element-free Galerkin methods for crack tip fields. *International Journal for Numerical Methods in Engineering,* 40: 1483-1504.

Gaul, L.; Kögl, M.; Wagner, M. (2003): *Boundary Element Methods for Engineers and Scientists*. Springer-Verlag, Berlin.

Hosseini-Tehrani, P.; Eslami, M.R. (2000): BEM analysis of thermal and mechanical shock in a two-dimensional finite domain considering coupled thermoelasticity. *Engineering Analysis with Boundary Elements*, 24: 249-257.

Houbolt, J.C. (1950): A recurrence matrix solution for the dynamic response of elastic aircraft. *Journal of Aeronautical Sciences*, 17: 371-376.

Kögl, M.; Gaul, L. (2003): A boundary element method for anisotropic coupled thermoelasticity. *Arch. Appl. Mech.*, 73: 377-398.

Krongauz, Y.; Belytschko, T. (1998): EFG approximation with discontinuitous derivatives. *Int. J. Numer. Meth. Engn.*, 41: 1215-1233.

Lekhnitskii, S.G. (1963): *Theory of Elasticity of an Anisotropic Body*. Holden Day, San Francisco.

Li, Q.; Shen, S.; Han Z.D.; Atluri, S.N. (2003): Application of meshless local Petrov-Galerkin (MLPG) to problems with singularities, and material discontinuities, in 3-D elasticity. *CMES: Computer Modeling in Engineering & Sciences*, 4: 571-585.

Mak, A.F.; Keer, L.M.; Chen, S.H.; Lewis, J.L. (1980): A no-slip interface crack. *ASME Journal of Applied Mechanics,* 47: 347-350.

Murakami, Y. (ed.) (1987): *Stress Intensity Factor Handbook.* Pergamon Press.

Nie, Y.F.; Atluri, S.N.; You, C.W. (2006): The optimal radius of the support of radial weights used in Moving Least Squares approximation. *CMES: Computer Modeling in Engineering & Sciences*, 12 (2): 137-147.

Nowacki, W. (1986): *Thermoelasticity*. Pergamon, Oxford.

Park, K.H.; Banerjee, P.K. (2002): Two- and three-dimensional transient thermoelastic analysis by BEM via particular integrals. *Int. J. Solids and Structures*, 39: 2871-2892.

Rice, J.R.; Sih, G.C. (1965): Plane problems of cracks in dissimilar media. *ASME Journal of Applied Mechanics*, 32: 418-423.

Sellountos, E.J.; Vavourakis, V., Polyzos, D. (2005): A new singular/hypersingular MLPG (LBIE) method for 2D elastostatics. *CMES: Computer Modeling in Engineering & Sciences*, 7: 35-48.

Sellountos, E.J.; Sequeira, A.; Polyzos, D. (2009): Elastic transient analysis with MLPG (LBIE) method and local RBF's. *CMES: Computer Modeling in Engineering & Sciences*, 41: 215-241.

Shiah, Y.C.; Tan, C.L. (1999): Exact boundary integral transformation of the thermoelastic domain integral in BEM for general 2D anisotropic elasticity. *Computational Mechanics*, 23: 87-96.

Sih, G.C.; Rice, J.R. (1964): The bending of plates of dissimilar materials with cracks. *ASME Journal of Applied Mechanics*, 31: 477-482.

Sinclair, G.B. (1980): On the stress singularity at an interface crack. *Int. Journal of Fracture,* 16: 111-119.

Sladek, V.; Sladek, J. (1984): Boundary integral equation method in thermoelasticity. Part I: General analysis. *Appl. Math. Modelling*, 7: 241-253.

Sladek, J.; Sladek, V.; Atluri, S.N. (2000): Local boundary integral equation (LBIE) method for solving problems of elasticity with nonhomogeneous material properties. *Computational Mechanics*, 24: 456-462.

Sladek, J.; Sladek, V.; Atluri, S.N. (2001): A pure contour formulation for meshless local boundary integral equation method in thermoelasticity. *CMES: Computer Modeling in Engineering & Sciences*, 2: 423-434.

Sladek, J.; Sladek, V.; Zhang, Ch. (2003a): Transient heat conduction analysis in functionally graded materials by the meshless local boundary integral equation method. *Computational Mechanics of Materials*, 28: 494-504.

Sladek, J.; Sladek, V.; Krivacek, J.; Zhang, Ch. (2003b): Local BIEM for transient heat conduction analysis in 3-D axisymmetric functionally graded solids. *Computational Mechanics*, 32: 169-176.

Sladek, J.; Sladek, V.; Atluri, S.N. (2004a): Meshless local Petrov-Galerkin method for heat conduction problem in an anisotropic medium. *CMES: Computer Modeling in Engineering & Sciences*, 6: 309-318.

Sladek, J.; Sladek, V.; Atluri, S.N. (2004b): Meshless local Petrov-Galerkin method in anisotropic elasticity. *CMES: Computer Modeling in Engineering & Sciences*, 6: 477-489.

Sladek, V.; Sladek, J.; Tanaka, M.; Zhang, Ch. (2005): Transient heat conduction in anisotropic and functionally graded media by local integral equations.

Engineering Analysis with Boundary Elements, 29: 1047-1065.

Sladek, J.; Sladek, V.; Zhang, Ch.; Tan C.L. (2006): Meshless local Petrov-Galerkin Method for linear coupled thermoelastic analysis. *CMES: Computer Modeling in Engineering & Sciences,* 16: 57-68.

Sladek, J.; Sladek, V.; Hellmich, Ch.; Eberhardsteiner, J. (2007): Heat conduction analysis of 3D axisymmetric and anisotropic FGM bodies by meshless local Petrov-Galerkin method. *Computational Mechanics,* 39: 2007, 323-333.

Sladek, J.; Sladek, V.; Tan C.L.; Atluri, S.N. (2008a): Analysis of transient heat conduction in 3D anisotropic functionally graded solids by the MLPG. *CMES: Computer Modeling in Engineering & Sciences,* 32: 161-174.

Sladek, J.; Sladek, V.; Solek, P.; Wen, P.H. (2008b): Thermal bending of Reissner-Mindlin plates by the MLPG. *CMES: Computer Modeling in Engineering & Sciences,* 28: 57-76.

Sladek, J.; Sladek, V.; Solek, P.; Wen, P.H.; Atluri, S.N. (2008c): Thermal analysis of Reissner-Mindlin shallow shells with FGM properties by the MLPG. *CMES: Computer Modeling in Engineering & Sciences,* 30: 77-97.

Suh, I.G.; Tosaka, N. (1989): Application of the boundary element method to 3-D linear coupled thermoelasticity problems. *Theor. Appl. Mech.*, 38: 169-175.

Tan, C.L.; Gao, Y.L.; Afagh, F.F. (1992): Boundary element analysis of interface cracks between dissimilar anisotropic materials. *Int. J. Solids and Structures*, 29: 3201-3220.

Yuuki, R.; Cho, S.B. (1989): Efficient boundary element analysis of stress intensity factors for interface cracks in dissimilar materials. *Engineering Fracture Mechanics*, 34: 179-188.

Wang, D.; Sun, Y.; Li, L. (2009): A discontinuous Galerkin meshfree modeling of material interface. *CMES: Computer Modeling in Engineering & Sciences*, 45: 57-82.

Williams M.L. (1959): The stresses around a fault or crack in dissimilar media. *Bull. Seism. Soc. Am.*, 49: 199-204.

Wu, X.H.; Shen, S.P.; Tao, W.Q. (2007): Meshless local Petrov-Galerkin collocation method for two-dimensional heat conduction problems. *CMES: Computer Modeling in Engineering & Sciences*, 22: 65-76.

Wünsche, M.; Zhang, Ch.; Sladek, J.; Sladek, V.; Hirose, S.; Kuna, M. (2009): Transient dynamic analysis of interface cracks in layered anisotropic solids under impact loading. *Int. Journal of Fracture*, 157: 131-147.

Zhang, Ch. (2005): Transient dynamic crack analysis in anisotropic solids. **In: Ivankovic A, Aliabadi MH** (eds.) *Crack Dynamics*, WIT Press, Southampton, pp.

71-120.

Zhu, T.; Zhang, J.D.; Atluri, S.N. (1998): A local boundary integral equation (LBIE) method in computational mechanics, and a meshless discretization approaches. *Computational Mechanics*, 21: 223-235.

Appendix

The constants d_α, t_α (α=1,2) and the bi-material constant ε are determined by

$$d_\alpha = G_\alpha(\cos\ \theta + 2\varepsilon\ \sin\ \theta) + P_\alpha(\sin\ \theta - 2\varepsilon\ \cos\ \theta), \tag{A.1}$$

$$t_\alpha = G_\alpha(2\varepsilon\ \cos\ \theta - \sin\ \theta) + P_\alpha(\cos\ \theta + 2\varepsilon\ \sin\ \theta), \tag{A.2}$$

$$\varepsilon = \frac{1}{2\pi}\ln\frac{1-\beta}{1+\beta}, \tag{A.3}$$

where

$$\begin{bmatrix} G_1 - iP_1 \\ G_2 - iP_2 \end{bmatrix} = g \begin{bmatrix} \frac{H_{12}}{H_{22}} - i\frac{\sqrt{H_{11}H_{22}-H_{12}^2}}{H_{22}} \\ 1 - 0 \end{bmatrix}, \tag{A.4}$$

$$g = \frac{H_{11}H_{22}(1-\varsigma^2) - H_{12}^2}{2\sqrt{H_{11}H_{22}-H_{12}^2}}, \tag{A.5}$$

$$\theta = \varepsilon\ \log\left(\frac{r}{l_r}\right), \quad \beta = \varsigma\frac{\sqrt{H_{11}H_{22}}}{\sqrt{H_{11}H_{22}-H_{12}^2}}, \tag{A.6}$$

$$\varsigma = \frac{[b_{11}(\eta_1\eta_2 - \xi_1\xi_2) - b_{12}]_I - [b_{11}(\eta_1\eta_2 - \xi_1\xi_2) - b_{12}]_{II}}{\sqrt{H_{11}H_{22}}}, \tag{A.7}$$

$$H_{11} = [b_{11}(\xi_1 + \xi_2)]_I + [b_{11}(\xi_1 + \xi_2)]_{II}, \tag{A.8}$$

$$H_{22} = \left[b_{22}\left(\frac{\xi_1}{\eta_1^2 + \xi_1^2} + \frac{\xi_2}{\eta_2^2 + \xi_2^2}\right)\right]_I + \left[b_{22}\left(\frac{\xi_1}{\eta_1^2 + \xi_1^2} + \frac{\xi_2}{\eta_2^2 + \xi_2^2}\right)\right]_{II}, \tag{A.9}$$

$$H_{12} = [b_{11}(\eta_1\xi_2 + \eta_2\xi_1)]_I + [b_{11}(\eta_1\xi_2 + \eta_2\xi_1)]_{II}. \tag{A.10}$$

In Eq. (A.6), r is the polar coordinate with the origin at the crack-tip and l_r is a reference length which is taken as the crack-length in the present analysis. Further η_α are the real part and ξ_α the imaginary part of the complex root μ_α and the subscripts I and II in Eqs. (A.7)-(A.10) indicate the material I and the material II.